Convection–Evaporation Feedback in the Equatorial Pacific

GUANG JUN ZHANG AND V. RAMANATHAN

Center for Clouds, Chemistry and Climate, and California Space Institute, Scripps Institution of Oceanography, University of California, San Diego, La Jolla, California

MICHAEL J. MCPHADEN

Pacific Marine Environmental Laboratory, National Oceanic and Atmospheric Administration, Seattle, Washington

(Manuscript received 21 December 1994, in final form 4 May 1995)

ABSTRACT

The coupling between convection and surface evaporation is investigated to assess the importance of evaporative cooling in regulating the tropical sea surface temperature. It is found that such a coupling is scale dependent. On timescales of several days, convective activity enhances surface evaporation, which together with the decrease of surface solar radiation, acts to cool the sea surface. However, on scales of climatic interest, convection acts to reduce surface evaporation. High sea surface temperature gives rise to more convective activity, which through interaction with the large-scale circulation, increases the low-level large-scale convergence and decreases the surface wind, leading to low evaporation in spite of the increased surface–air humidity difference. Therefore, although individual convective events can significantly enhance surface evaporation on short timescales, the long-term average effect of convection is to suppress surface evaporation at high SST due to its interaction with the large-scale circulation. One potential implication of this result is that evaporative cooling on climate timescales may not provide a negative feedback on the sea surface temperature of warm oceans with convectively disturbed tropospheres.

1. Introduction

What processes control tropical western Pacific sea surface temperature (SST)? How important is convection in these processes and through what mechanisms? These questions are germane to many important climate issues. In an attempt to explain the apparent upper limit of SST in the tropical western Pacific, Ramanathan and Collins (1991) proposed a "thermostat hypothesis" that invokes the shielding effect of thick cirrus clouds. According to their hypothesis, as SST increases above a threshold value, convection starts to develop; a further increase in SST leads to more convection. The convectively generated optically thick anvil clouds cover a large area, keeping the solar radiation from reaching the sea surface, thus effectively cooling the ocean.

Ramanathan and Collins's paper has provoked many interesting debates on what processes regulate SST. For instance, Wallace (1992) suggests that evaporative cooling is a more competitive candidate to regulate the tropical western Pacific SST. According to his argument, increase in SST leads to enhanced heat exchange (through sensible and latent heat fluxes) between the atmospheric boundary layer and the ocean, which cools the ocean surface. The excess energy in the atmospheric boundary layer is then carried upward by convection to the upper troposphere, and further carried away by large-scale circulation to the eastern Pacific.

The premise of Wallace's argument is that surface evaporation increases with SST, which is a natural conclusion from thermodynamic considerations. Recently, by assuming (essentially) a constant wind speed and a constant relative humidity in the bulk aerodynamic formula for surface latent heat flux, Hartmann and Michelsen (1993) estimated that the increase of latent heat flux with SST is about 7.2 W m^{-2} K^{-1}, which exceeds the atmospheric longwave super greenhouse effect. Thus, they conclude that evaporative cooling is a dominant limiting factor in determining tropical SST.

The argument that high SST should lead to enhanced surface evaporation is at variance with the observations. Cornejo-Garrido and Stone (1977) were perhaps the first to notice the negative correlation between SST and surface evaporation in the tropical western Pacific when examining the surface heat budget to investigate the driving force of the Walker circulation. Using the daily data from TAO (Tropical Atmosphere–Ocean) moored buoys deployed in the equatorial Pacific (8°N–8°S, 137°E–95°W) from 1991 to 1993, Zhang and McPhaden (1995) analyzed surface latent heat flux

Corresponding author address: Dr. Guang Jun Zhang, California Space Institute, Scripps Institution of Oceanography, University of California, San Diego, La Jolla, CA 92093-0221.

computed from the bulk formulas. They found that the relationship between latent heat flux and SST is more complex than the simple monotonic increase as suggested in Hartmann and Michelsen (1993). In the equatorial Pacific, for SSTs less than about 300–301 K, latent heat flux increases with SST at a rate of about 12 W m^{-2} K^{-1}, of which about 2 W m^{-2} K^{-1} is from the contribution of wind speed change and 10 W m^{-2} K^{-1} is from the contribution of humidity deficit change with SST. On the other hand, for SSTs greater than this threshold value, the daily averaged latent heat flux actually decreases with SST at about -10 W m^{-2} K^{-1}, of which wind speed change and humidity deficit change contribute -25 W m^{-2} K^{-1} and 15 W m^{-2} K^{-1}, respectively. Note that at low SSTs the change of latent heat flux with SST is dominated by the contributions from the humidity deficit or thermodynamics, whereas at high SSTs it is dominated by the contributions from the wind speed or dynamics, although the thermodynamic contribution is consistent with the argument of Hartmann and Michelsen (1993). Figure 1 shows the cumulative frequency distribution of surface latent heat flux and wind speed, obtained from the daily TAO buoy data of Zhang and McPhaden (1995), as a function of SST binned at each 1 K interval. Each contour represents the percentage of the observations having latent heat flux less than a particular value at a given SST. High latent heat flux is observed more frequently near 300–301 K than elsewhere. For example, at 296 K, only about 1% of the samples have evaporation (E) in excess of 100 W m^{-2}; between 300 and 301 K, more than 50% of the samples have $E > 100$ W m^{-2}. As SST increases, the frequency of high latent heat flux decreases, with, for example, $E > 100$ W m^{-2} only 30% of the time for SSTs of 303 K. It is interesting to note that very high latent heat fluxes, which might be associated with systems such as strong westerly wind bursts, are not observed frequently. For example, only less than 10% of the samples of the observed latent heat flux exceed 150 W m^{-2}.

From the cumulative frequency distribution for surface wind speed (Fig. 1b), it is evident that surface winds decrease sharply with SST at high SSTs: at 300–301 K, about 50% of the observed wind speeds are more than 6 m s^{-1}, whereas for SSTs > 302 K, less than 20% of the observed winds exceed this value, an impressive decrease in the frequency of occurrence of high wind speeds. Meanwhile, the frequency of occurrence of low wind speeds experiences substantial increase. At 300 K, less than 5% of the observed winds are weaker than 2 m s^{-1}, whereas for SSTs > 302 K more than 20% of the observed winds are weaker than 2 m s^{-1}. Clearly, suppression of surface latent heat flux at high SSTs is at least in part a result of decreasing surface wind speed. This relationship between SST and surface wind speed is generally overlooked by those investigators who emphasize the importance of evaporative cooling in limiting the maximum tropical SST.

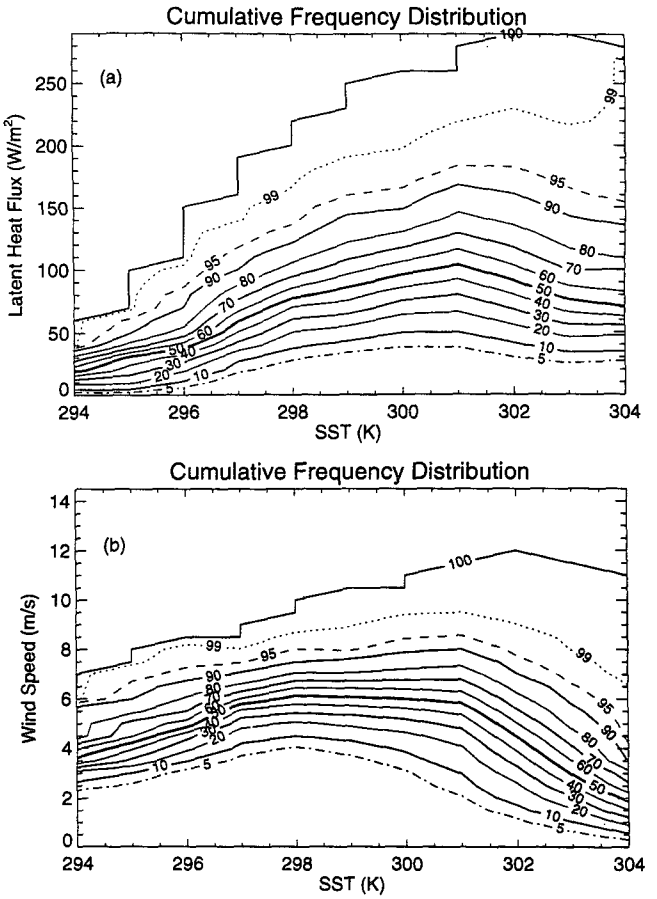

FIG. 1. Cumulative frequency distribution (%) of (a) latent heat flux (W m^{-2}) and (b) surface wind speed (m s^{-1}) as functions of SST (K).

To understand why surface evaporation is relatively low at high SST, we must first answer the question why wind speed is low at high SST, and what physical processes link them? Since the threshold SST for convection is about 300 K (e.g., Graham and Barnett 1987), the same value at which wind speed starts to decrease with SST, we anticipate convection to be an important factor in the mechanisms that associate low wind speed with high SSTs. Thus, the objective of this study is to understand the role of convection in the observed relationships between surface wind speed, latent heat flux, and SST.

Cumulus convection affects surface evaporation by modifying the boundary layer properties near the surface. Convective-scale updrafts and downdrafts transport the warm and moist surface air into the upper troposphere and the cold, dry midtropospheric air into the boundary layer. As a result, the air–sea temperature and moisture difference is increased. Accompanying the convective activity, surface wind is often increased substantially as well. These dynamic and thermodynamic changes frequently lead to enhanced surface

evaporation. Such enhancement in convective regions was documented by Young et al. (1992) and Parsons et al. (1994) in the tropical western Pacific and by earlier studies in other regions of the Tropics (Gaynor and Ropelewski 1979; Johnson 1981). In this study, we will address the interaction between convection and surface evaporation on timescales from several days (pertinent to weather) to a few months and longer (pertinent to climate), so as to provide some insight into the integrated effect of convection on surface evaporation. We will also discuss the implication of the results to the regulation of the tropical sea surface temperature.

2. Data and data processing

In situ data used in this study are derived from the TAO array, which consists of approximately 70 deep-ocean moorings spanning the equatorial Pacific Ocean between 8°N and 8°S, 95°W and 137°E (McPhaden 1993). The purpose of the array is to provide high quality, in situ, real-time data in the equatorial Pacific Ocean for short-term climate studies, most notably those relating to the El Niño–Southern Oscillation phenomenon. The array is supported by a multinational effort involving institutions in the United States, Japan, Korea, Taiwan, and France. TAO measurements consist of surface winds, sea surface temperature, upper-ocean temperature and currents, air temperature, and relative humidity. Recently, additional sensors have been added for incoming shortwave radiation (Eppley PSP pyranometers), rainfall (Scientific Technology, Inc., mini-optical rain gauges), and salinity (SeaBird SEACATS). Daily averaged data are telemetered in real time via Service Argos, and a subset of these data is placed on the Global Telecommunications System for distribution to operational centers for assimilation into weather and climate forecast models. On recovery, internally recorded hourly data and, in the case of shortwave radiation, 20-min data are available for analysis. Accuracy of the basic measurements is discussed in Mangum et al. (1994), Freitag et al. (1994), and Short et al. (1994). Latent heat fluxes are computed from the wind, SST, air temperature, and relative humidity measurements as in Zhang and McPhaden (1995) using a bulk formula similar to that in Liu et al. (1979).

The outgoing longwave radiation (OLR) data used in this study are from Advanced Very High Resolution Radiometers on National Oceanic and Atmospheric Administration polar orbiters, archived at the National Meteorological Center (NMC). They cover the period from 1 January 1992 to 30 May 1993, at 5-day resolution in time and 2.5° × 2.5° in space. The OLR grid cells are collocated with the buoy positions when variables from the two datasets are compared.

The NMC optimally interpolated weekly SST is also used in this study. This dataset uses in situ and satellite SST plus SSTs simulated by sea ice cover. Details of the analyses are described in Reynolds and Smith (1994).

3. Short timescale feedback

The fields used in this section include daily averaged SST, latent heat flux, surface solar radiative flux, and precipitation. To focus on the short timescale variations, each time series is high-pass filtered to remove the intraseasonal and lower-frequency variations while keeping the signals of shorter timescales, such as synoptic-scale weather systems, which have a timescale of about a week. The filter is implemented by first low passing the time series with a 25-day running mean, then subtracting the low-passed time series from the original data. The choice of the width of the running mean window (25 days) is based on a power spectrum analysis of the time series, which shows a minimum energy density at 25-day periods. All the data used in this section are high-pass filtered, that is, deviations from the 25-day running means, except precipitation, which is more indicative of convection in its entirety.

Figure 2 shows the time series of the deviations from the running means of SST, latent heat flux, surface solar radiation, surface wind speed, and total precipitation from September to December 1992 at 0°, 156°E. The precipitation data is used here mainly to identify convection rather than to quantify rainfall totals. Several of the variables show significant correlation. For instance, variations of latent heat flux and solar radiation are of comparable magnitude but are generally out of phase; SST is negatively correlated with surface latent heat flux but positively correlated with solar radiation; variations of latent heat flux are dominated by variations in surface wind speed. To quantify the relationships between the different variables, data from the two buoys that have both rainfall rate and solar radiation data are used (0°, 156°E already described and 0°, 165°E). Table 1 presents the cross-correlation estimates among SST, wind speed, latent heat flux, and solar radiation from these buoys. A maximum negative correlation coefficient of −0.42 (with a 95% confidence value of −0.17) between SST and latent heat flux (similar for wind speed) is found when SST lags by one day. A maximum negative correlation coefficient of −0.44 is found between latent heat flux and surface solar radiation at zero lag. It is interesting to note that using the buoy data from 0°, 165°E covering the period December 1986–October 1987, McPhaden and Hayes (1991) found a similar degree of correlation between SST and wind speed: a correlation coefficient of −0.52, with SST lagging wind speed by 1 day. Other qualitative features seen in the time series are all manifested in Table 1 by the significant correlation coefficients.

To examine the influence of convection on the surface fluxes and wind speed, we take the approach of

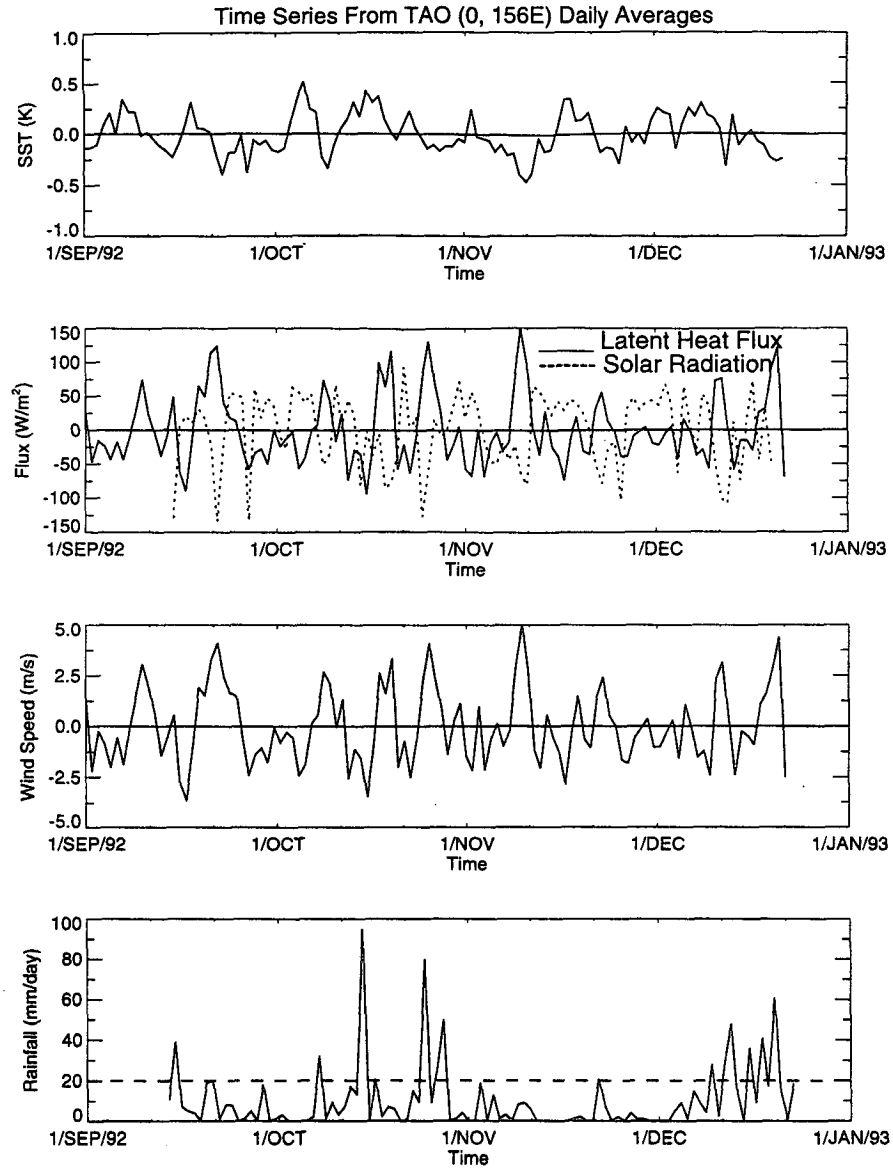

FIG. 2. Time series of the deviations from the 25-day running mean for SST (K, top panel), latent heat flux and solar radiative flux (solid line and dashed line, respectively; units: W m^{-2}; second panel), and wind speed (m s^{-1}, third panel). The bottom panel is the time series of the total precipitation (mm day^{-1}).

Young et al. (1992), who used rainfall rate in conjunction with cloud-type observations to stratify the surface data collected during a 22-day cruise in the western Pacific warm pool. However, since we do not have cloud-type observations, we will use rainfall rate alone as an indicator of convective activity. This may not work well at times when deep convection is present without precipitation being registered at the buoy sites. But as we will see shortly, solar radiation, which is strongly influenced by cloud cover, is well separated from one category to another so devised. For precipitating convection, we consider days with rainfall rate of 20 mm day^{-1} as the boundary between intense and moderate convection (use of a different value does not affect the results qualitatively). Tables 2 and 3 give the mean values of SST, wind speed, latent heat flux, solar radiation deviations, and the total rainfall rate in each category for the two buoys at 0°, 156°E and 0°, 165°E. The second column in each table gives the number of days each category is observed. The large differences in mean solar radiation from one category to another, together with those in rainfall rates, clearly indicate the

TABLE 1. Extrema in cross correlations between variables in Fig. 2. For extrema at nonzero lags, the lags (with columns leading rows in days) are indicated in parentheses. All correlations given are significant at the 95% confidence level.

	SST	Wind speed	Latent heat flux	Solar radiation
SST	1.0	−0.45 (+1)	−0.42 (+1)	0.46
Wind speed		1.0	0.97	−0.40
Latent heat flux			1.0	−0.44
Solar radiation				1.0

differences in convective activity and support the validity of the classification.

The variation of solar radiation reflects the cloudiness in the free atmosphere, whereas that of surface latent heat flux reflects the surface dynamic and thermodynamic conditions. The coupling between the two is apparently through convection. When convection occurs, clouds associated with the convective system block the solar radiation from reaching the surface, thus reducing the surface solar radiation. At the same time, convection-generated cold, dry air and high wind on the surface, especially the latter, act to enhance the surface evaporation, as also observed by Young et al. (1992) and Parsons et al. (1994). The stronger the convection, the larger the convective effects on surface winds, latent heat flux, and solar radiation. On the other hand, clear sky and fair weather are associated with higher solar radiation, lower surface winds, and latent heat flux (negative deviations from the means). SST is generally warmer under clear skies and colder convective conditions.

Figure 2 and Tables 1, 2, and 3 illustrate the short timescale SST response to atmospheric forcing associated with convection, in which surface evaporation and shortwave cloud radiative forcing act *cooperatively* to affect SST variations. When the sky is clear (cloudy), surface solar radiation is high (low), and surface wind is weak (strong), thus latent heat flux is low (high). As a result, the ocean experiences a net heating (cooling), which leads to an increase (decrease) of SST. Thus, both surface evaporation and shortwave cloud radiative forcing provide a negative feedback on SST variation on such timescales.

4. Climate timescale feedback

The climate-scale variations of SST, wind speed, and latent heat flux, and their relationships will be examined in this section. For this purpose, latent heat flux and SST data from TAO buoys covering 1991–93 are used. Solar radiation data from the buoys cover only a few months, not long enough for studies of climatic scales, and thus will not be used in this section. Instead, the OLR data from satellite collocated with the buoys will be used as a surrogate for convective activity. The excellent correspondence between OLR and solar irradiance measured from TAO buoys is discussed in Kessler and McPhaden (1995), so that for our purposes these two datasets can be thought of as interchangeable.

a. Spatial and temporal variations

Figure 3 shows the scatterplots of wind speed, humidity difference between surface air and saturation humidity at SST (hereafter referred to as humidity deficit), and latent heat flux versus SST, averaged over the record length. Each point on the plot represents a different buoy. Also shown are the theoretical values of the humidity deficit as functions of SST for constant relative humidity (dotted curve) and constant specific humidity at 300 K (dashed curve), respectively. The prescribed values for relative humidity (81.5%) and specific humidity (18 g kg^{-1}) are obtained from the average of the buoy data. The average wind speed remains essentially constant for SST below 301 K, then experiences a sharp decrease for higher SST, similar to the pattern noticed in Fig. 1. The humidity deficit in general increases with SST everywhere, in agreement with the theoretical considerations. The average latent heat flux follows the trend of humidity deficit, increasing with SST up to a point. However, it levels off and then trends downward for SST $\geq$ 302 K, in spite of the increase in humidity deficit. This is clearly a result of the negative correlation of wind speed with SST for SST $>$ 301 K.

Another way to study the relationships between the variables is to examine if the *changes* of SST and the *changes* of other quantities in time are related. For instance, if SST at a given location undergoes a warming, would wind speed also undergo a change accordingly?

TABLE 2. Mean values of surface variables stratified by rainfall rate at 0°, 156°E. As described in the text, time series have been high-pass filtered and SST has been lagged by one day to maximize correlation with surface meteorological data.

	Number of days	SST (K)	Wind speed (m s^{-1})	Latent heat flux (W m^{-2})	Solar radiation (W m^{-2})	Rainfall (mm day^{-1})
No precipitation	31	0.091	−0.99	−26.8	21.9	0.
Precipitation <20 mm day^{-1}	52	−0.049	0.43	11.7	−2.1	7.1
Precipitation >20 mm day^{-1}	14	−0.032	0.71	24.2	−48.8	43.2

The time rate of change of variable X is computed by

$$\frac{\delta X(t)}{\delta t} = \frac{X(t + \delta t/2) - X(t - \delta t/2)}{\delta t},$$

where X is a meteorological variable of concern, such as SST or latent heat flux from the original data; t is time, and δt is the time interval at which the difference is taken. Here, $\delta t = 2$ days is used. The changes so obtained contain high-frequency noise and must be filtered to get climate-scale signals. For this purpose, a low-pass running mean filter is applied to each time series. Cutoff periods of 30, 60, and 90 days are tested, and it is found that while results from 60 and 90 day cutoff times are quite similar there is some noticeable difference when a 30-day cutoff time is used. This is due to contamination by 30–60 day waves in the tropical Pacific. On such intraseasonal timescales, evaporation forces SST change in the western Pacific, with evaporation leading by 10–15 days (Zhang and McPhaden 1995). Since we are interested in relationships between changes in SST, wind speed, and latent heat flux on climate timescales, a 60-day cutoff time is used for the time filter. A longer cutoff time could also be used, but this would reduce the independent sample size. Furthermore, 60 days is also roughly the timescale needed for the tropical Pacific Ocean mixed layer to respond to the surface forcing (Liu 1988; Liu and Gautier 1990; Arking and Ziskin 1994).

Based on the previous figures, variations of wind speed and latent heat flux with SST can be examined in three different SST regimes. For SST < 299 K, latent heat flux is expected to increase with SST; the 299 K < SST < 301 K region may be considered as a transition regime, where no significant relationship between SST and wind speed or latent heat flux is expected; for SST > 301 K, a negative relationship is expected. Figure 4 shows δU (change of wind speed) as functions of δT_s (change in SST) in the three SST regimes, respectively. The changes of wind speed are binned according to SST changes at 0.2 K per 10-day interval (note that the figures are scaled up by a factor of 10, so the changes are per 10 days). For SSTs < 299 K, changes of wind speed are essentially independent of SST changes, implying warming or cooling in cold waters is not related to changes in wind speed, and vice versa. For SSTs > 299 K, cooling is accompanied by an increase in wind speed and warming is accompanied by a decrease in wind speed, but the slope is smaller at SSTs between 299 and 301 K. For SSTs > 301 K, the slope is larger, except for large positive SST changes, where wind speed decrease is only moderate. For comparison, Fig. 5 shows changes of humidity deficit as functions of SST changes in the three SST regimes. The slopes between the changes of humidity deficit and those of SST are positive in all three SST regimes,

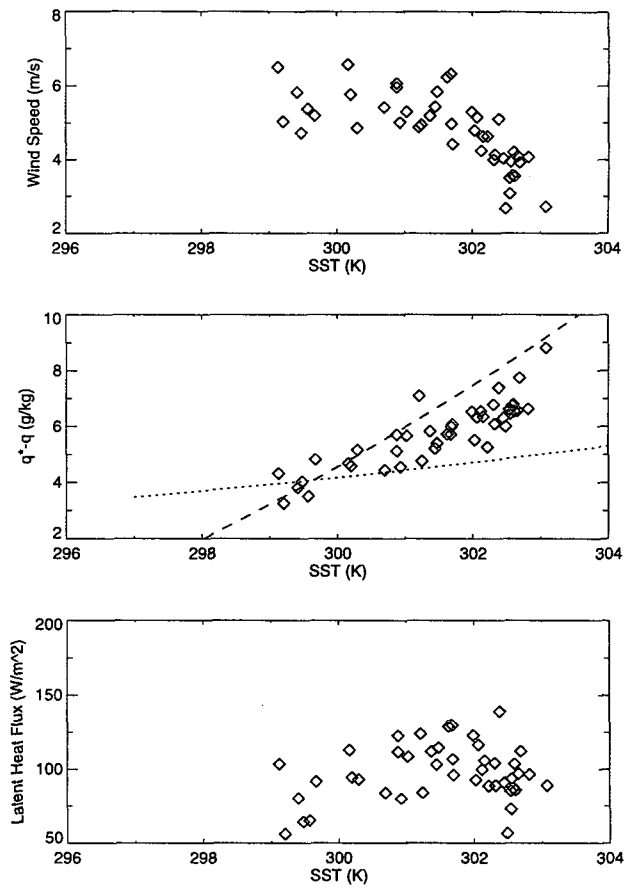

FIG. 3. Wind speed (m s^{-1}, top panel), humidity deficit $q_s - q$ (g kg^{-1}, middle panel), and latent heat flux (W m^{-2}, bottom panel) as functions of SST, averaged over the record length. Each point on the plot represents a different buoy. In the middle panel, the dashed line is the theoretical value of $q_s - q$ for fixed q at 300 K air temperature; the dotted line is for fixed relative humidity.

TABLE 3. Same as Table 2 except at 0°, 165°E.

	Number of days	SST (K)	Wind speed (m s^{-1})	Latent heat flux (W m^{-2})	Solar radiation (W m^{-2})	Rainfall (mm day^{-1})
No precipitation	19	0.040	−0.57	−11.9	16.1	0.
Precipitation < 20 mm day^{-1}	8	−0.069	0.49	10.1	−27.4	7.1
Precipitation >20 mm day^{-1}	7	−0.153	1.83	39.1	−51.6	50.7

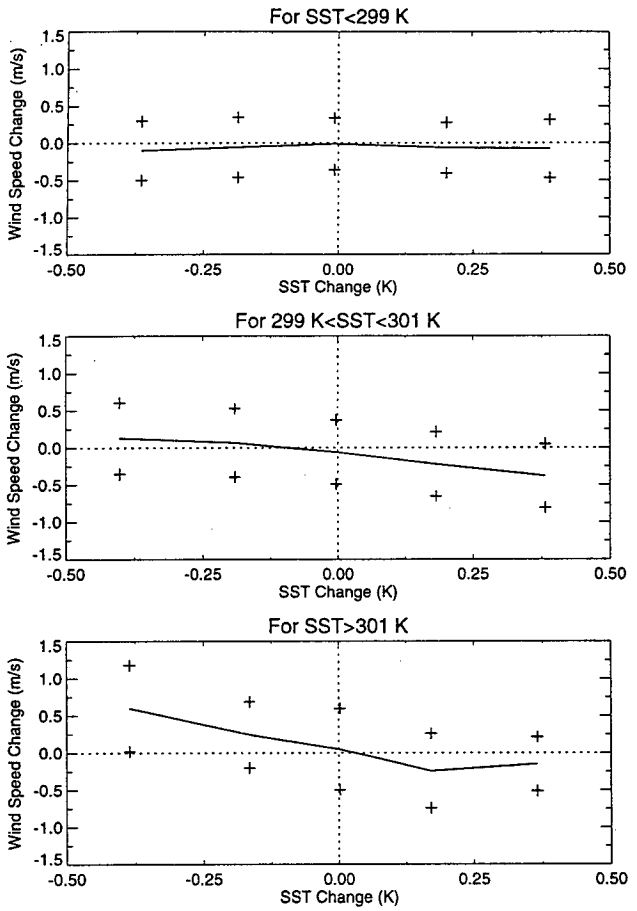

FIG. 4. Temporal changes of wind speed vs temporal changes of SST per 10 days, binned for 0.2-K interval, for SST < 299 K (top panel), 299 K < SST < 301 K (middle panel), and SST > 301 K (bottom panel). The solid line represents the average over the SST bin, and the + symbols give one standard deviation from the mean.

again consistent with thermodynamic considerations. In other words, warming is accompanied by increase in surface humidity deficit, and cooling is accompanied by decrease in humidity deficit.

Figure 6 shows the changes of latent heat flux against SST changes in the three SST regimes. The competing effects of wind speed and humidity deficit on the latent heat flux variation is clearly reflected in this figure. In the low SST regime, changes in latent heat flux during the warming and cooling periods are dominated by changes in humidity deficit, resulting in an increase in latent heat flux when warming occurs and a decrease in latent heat flux when cooling occurs. In the transition regime, the influence of wind speed change and humidity deficit changes is comparable, leaving essentially no relationship between changes in latent heat flux and changes in SST. In the high SST regime, the effect of wind speed is apparently dominant, leading to a negative slope, except for large positive SST changes, where a small wind speed decrease is not enough to compensate the large increase in humidity deficit, resulting in slight increase in evaporation. It should be pointed out that the patterns shown here are for the average. Individual warming or cooling periods may have considerable variance as indicated by relatively large standard deviations. Nevertheless, the above results do suggest that, at high SST, warming in SST is more frequently accompanied by decrease in evaporation, and cooling in SST is more frequently accompanied by increase in evaporation.

In summary, these results demonstrate that wind speed changes little with SST at low SSTs, but decreases significantly as SST increases at high SSTs. Hence, surface latent heat flux, which depends strongly on wind speed at high SST, on average does not increase with SST beyond 301 K.

The above conclusions are based on the contemporaneous binning between surface wind speed, humidity deficit, latent heat flux, and SST. Time lag relationships between these variables are also examined following the binning procedure of Arking and Ziskin (1994), with time lag from −4 months to 4 months, to investigate the question of whether the atmospheric surface

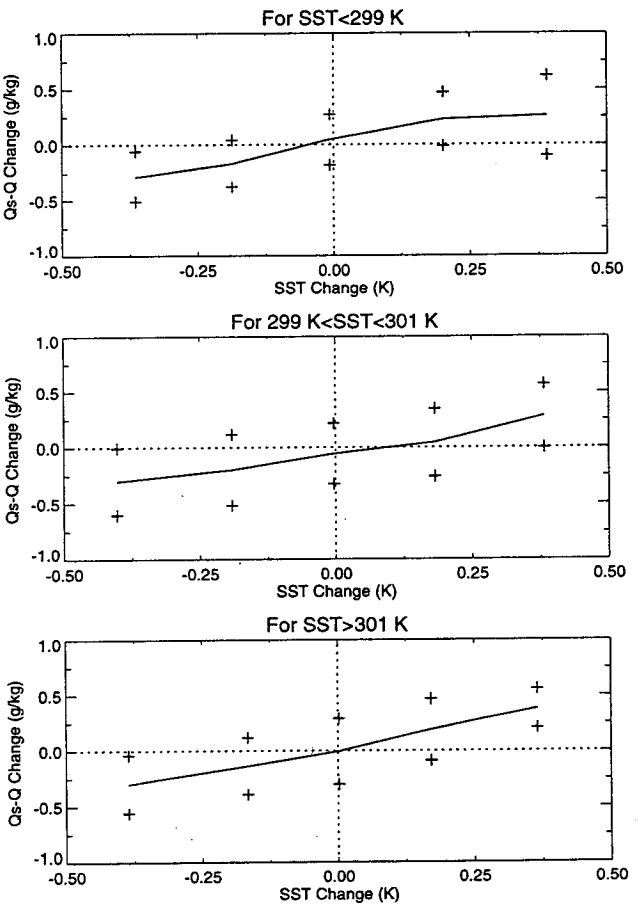

FIG. 5. Same as Fig. 4 but for changes of humidity deficit.

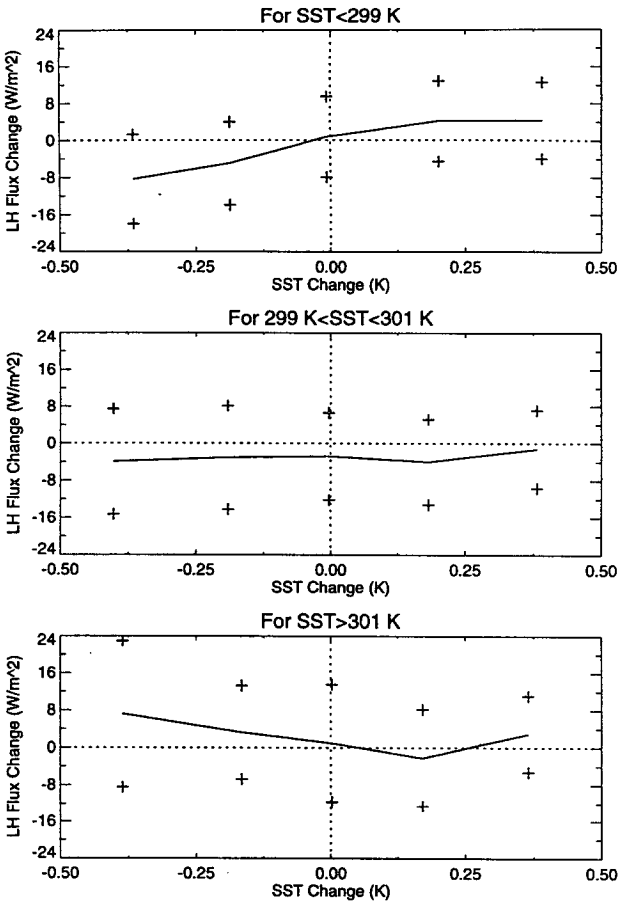

FIG. 6. Same as Fig. 4 but for changes of latent heat flux.

variables respond to SST or the other way round. The best relationship between SST and wind speed, and between SST and latent heat flux using the filtered data, is obtained at zero time lag. Furthermore, for all the time lags the relationship between wind speed and SST is significantly better than the relationship between latent heat flux and SST. The correlation between latent heat flux and SST change is low as well. According to Arking and Ziskin (1994), these results suggest that low wind speed is a direct response to high SST, and latent heat flux is linked to SST through the influence of SST on surface wind. In consideration of Figs. 3–6, the humidity contribution to the variation of surface evaporation with SST seems to have been overemphasized in the arguments that stress the importance of evaporative cooling in limiting the tropical SST.

b. Interaction between SST, convection, and large-scale dynamics

What causes the observed relationships between SST, surface wind, and latent heat flux, or more precisely, how are surface winds and latent heat flux affected by SST? The mechanism that we explore here is the interaction between SST, convection, and the large-scale dynamics. In such a mechanism, convection is crucial to linking SST and the low-level large-scale atmospheric flow, thus surface evaporation.

Numerous observational studies have indicated that convection is well related to SST in the tropical Pacific. Above the threshold of about 300–301 K in SST, the activity (intensity and/or frequency of occurrence) of large-scale convection increases with SST (Graham and Barnett 1987; Waliser and Graham 1993; Waliser et al. 1993; Zhang 1993). To examine the relationship between convection and SST during the period covered by the buoy observations, we use the NMC OLR data. OLR has been used in the past to infer convection (see references above): lower OLR corresponds to convectively active troposphere, and higher OLR corresponds to convectively suppressed troposphere. Although OLR may not always correctly represent the state of convective activities, it suffices for our purposes to use OLR as a proxy for convection.

Figure 7a shows the cumulative frequency distribution of pentad OLR as functions of pentad SST (av-

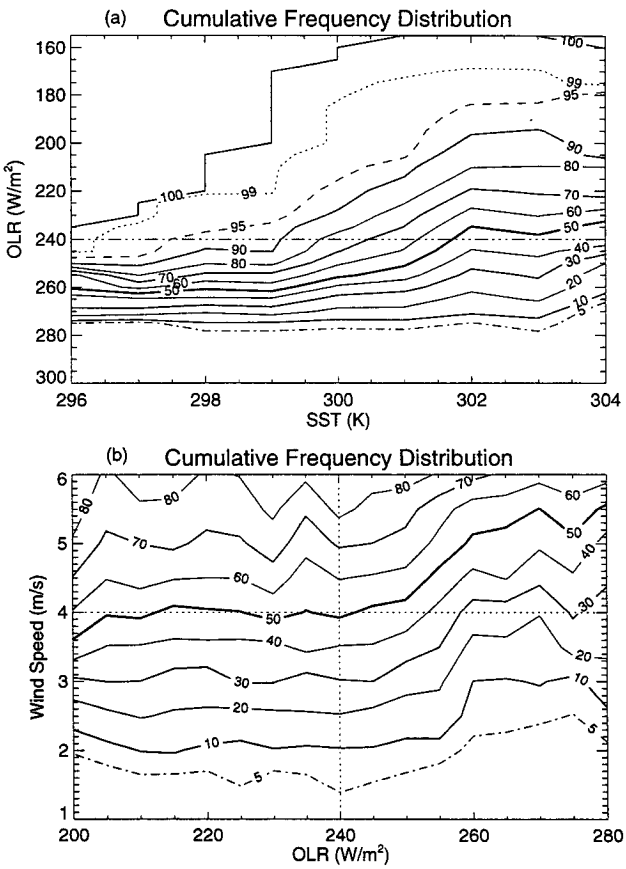

FIG. 7. Cumulative frequency distribution (%) of (a) OLR (W m^{-2}) as a function of SST (K) and (b) wind speed (m s^{-1}) as a function of OLR.

eraged using buoy data) for the period. If one adopts the customary use of 240 W m^{-2} OLR for convection, the following conclusions can be made: i) for SST < 300 K, convection is very infrequent, and ii) above 300 K, the frequency of convection increases significantly, from about 20% of the time at 300 K to more than 50% of the time at 302 K. Furthermore, above the 300–301-K threshold for convection, surface winds are distinctly different between convective and nonconvective regimes. Figure 7b shows the cumulative frequency distribution of wind speed as functions of OLR for SST > 300 K. It is evident that low wind speeds are observed much more frequently in convective regimes than in nonconvective regimes.

The above analyses of the buoy data and the OLR data suggest that high SSTs are associated with low surface wind speed and frequent convection. Therefore, at high SSTs when the atmosphere is convectively disturbed, surface evaporation is relatively suppressed due to low surface wind, despite a high humidity deficit resulting from the exponential increase of saturation water vapor pressure with SST. In summary, one plausible scenario is that higher SST leads to more convection, which in turn induces more low-level large-scale convergence; by its nature, this convergent wind field is associated with low horizontal wind speeds and low evaporation in regions of convection. Weak surface wind and strong low-level convergence in the tropical western Pacific, where deep convection is abundant, has been well simulated by several simple dynamic models that parameterize convection (Gill 1980; Lindzen and Nigam 1987; Wang and Li 1993).

c. *General circulation model simulation*

The postulated coupling between convection and the large-scale low level flow is further examined using an atmospheric general circulation model of the Max-Planck Institute for Meteorology, Germany (Reockner et al. 1992). The model is in spectral form, with an equivalent grid size of about 2.8° × 2.8°. The observed monthly averaged SST is used for the lower boundary conditions. Two one-year simulations are performed, one with a mass flux convective parameterization scheme (Zhang and McFarlane 1995) and one without convective parameterization. Thus, the difference between the two simulations measures the net (both direct and indirect) effect of convection. Figure 8 plots the surface wind speed, humidity deficit, and latent heat flux as functions of SST for the simulations with convection (open diamonds connected with a solid line) and without convection (open triangles) for the domain of (7°N, 7°S), (150°E, 110°W), about the same region covered by the moored buoys. Each point represents an average over a 0.5-K SST bin of the annually averaged SST from June 1985 to May 1986. In the simulation with parameterized convection, the variations of wind speed, humidity deficit, and latent heat flux with SST

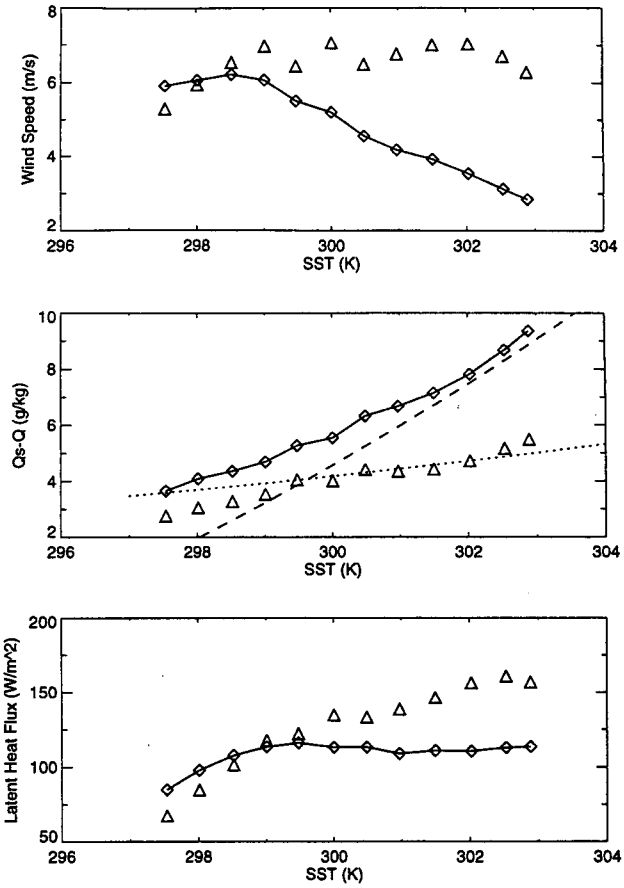

FIG. 8. Annually averaged wind speed (m s^{-1}, top panel), humidity deficit (g kg^{-1}, middle panel), and latent heat flux (W m^{-2}, bottom panel) as functions of SST for the simulations with convection (diamonds connected with solid line), and without convection (open triangles) for the domain of (7°N, 7°S), (150°E, 110°W), about the same region covered by the moored buoys. Each point represents an average over a 0.5-K bin. The dashed and solid lines in the middle panel are the same as in Fig. 3.

are very similar to those observed by the buoys (cf. Fig. 3). On the other hand, without convection, wind speed first increases with SST at low SSTs and then remains more or less constant at SSTs above 299 K, with a magnitude of 6–7 m s^{-1}. The humidity deficit in both the simulations increases with SST but at a lower rate without convection. The surface latent heat flux without convection is significantly higher at high SST, above 150 W m^{-2}. Furthermore, it increases with SST not only at low SSTs but also at high SSTs. For example, the latent heat flux increases from about 125 W m^{-2} at 299.5 K to more than 150 W m^{-2} at 303 K SST, at a rate very close to that obtained by Hartmann and Michelsen (1993) from thermodynamic considerations alone (7.2 W m^{-2} K^{-1}). From this comparison, it is evident that convection is associated with low wind speed, which in turn is responsible for the suppressed

latent heat flux at high SSTs, in spite of the high humidity deficit.

It is interesting to note that the humidity deficit in the convection case closely follows the constant specific humidity curve, whereas that without convection more follows the constant relative humidity curve for SSTs above 300 K; below 300 K they are quite close. This difference is due to the way in which moisture is removed from the surface boundary layer by convection and large-scale precipitation. Without convection, in order for large-scale condensation to occur, the air must reach a critical saturation value, regardless of SST. Thus, in the tropical western Pacific, where SST is above 300 K and large-scale dynamics favors uplifting, surface air naturally follows constant relative humidity. In the convective case, when surface humidity increases in response to SST increase, the surface air becomes more moist statically unstable, and convection ensues, transporting the excess moisture out of the boundary layer. Because of the efficient removal of surface moisture by penetrating convection, further increases in SST will not lead to significant increase in surface moisture content. The end result is that the surface specific humidity is close to that at 300 K SST, a threshold SST for convection onset.

The difference between low-level large-scale circulation with and without convection in the GCM is illustrated by Fig. 9, which plots the surface wind vectors averaged annually from the two simulations. In the convective case, surface winds are weak in the western Pacific warm pool as well as in the intertropical convergence zone and the South Pacific convergence zone, where the low-level convergence is strong. Without convection, strongest surface convergence is over the maritime landmass, and most of the central and western equatorial Pacific is dominated by strong easterlies. These stronger winds are partly due to the enhanced Walker circulation associated with more unstable thermodynamic stratification when the stabilizing effect of convection is absent (Zhang 1994). Such strong easterlies are required to supply moisture from the central and eastern Pacific for precipitation in the western end of the warm pool.

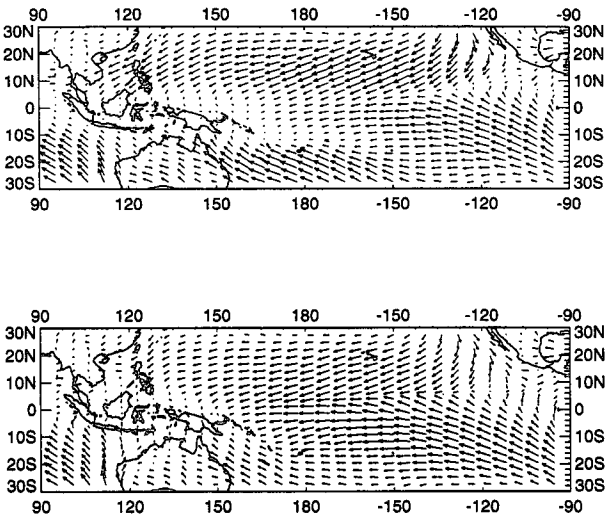

FIG. 9. Annually averaged wind vector fields from 30°N to 30°S for the simulations with convection (top panel) and without convection (bottom panel). Each vector of grid length represents 5 m s^{-1}. Vectors are plotted at every other grid point along the longitude axis.

5. Discussion and conclusions

This study attempts to investigate the coupling between convection and surface evaporation using TAO buoy data and numerical simulations from a general circulation model. The major findings are summarized below.

- Events of high latent heat flux (> 150 W m^{-2}) associated with high surface wind speed are not observed frequently. They account for less than 10% of the total observations during our 2-yr study.
- The frequency of occurrence of low wind speeds increases dramatically at high SSTs (>301 K), resulting in sharp decrease of the average wind speed with SST.
- On temporal scales of several days, convection enhances the surface evaporation via the increase of surface wind speed. On such timescales, evaporation and cloud solar radiative forcing act cooperatively to regulate the SST variation.
- On climate timescales (i.e., periods longer than about a month), the variation of latent heat flux at high SSTs is dominated by variations in wind speed. While changes of humidity deficit with SST are consistent with thermodynamic considerations, decreases in wind speed with SST lead to relatively suppressed latent heat flux at high SSTs.

Based on these results, the linkage between SST, convection, and surface evaporation is examined. On climate timescales, high SST leads to more convection, which increases the low-level convergence and decreases surface wind, resulting in suppressed latent heat flux in regions of convection. In the context of tropical SST regulation, this interaction between convection and large-scale circulation has not received much attention in the past and can well explain seemingly contradictory results from different observational studies. On the one hand, some measurements have been interpreted to imply that surface evaporation is enhanced by convection. Such ventilation and cooling effects of convection have been emphasized by several researchers (e.g., Lau and Sui 1993; Lau et al. 1994) when investigating the role of evaporative heat flux in regulating the SST. If the climatological effect of convection is to enhance the surface evaporation, one would expect high evaporation in regions where there is abundance of convection, such as the western Pacific warm pool. On the other hand, long-term observations and

climatological data suggest that these regions are dominated by low evaporation. From the analyses presented in this study, it is obvious that the enhancement on short timescales is a direct effect of convection, whereas suppression of evaporation on the climate scale is an indirect and dominant effect of convection, which involves the interaction between convection and the large-scale circulation. Therefore, *although individual convective events can enhance surface evaporation substantially on short temporal scales, the long-term average effect of convection is to suppress surface evaporation at high SST due to its interaction with the large-scale circulation.*

The coupling mechanism based on our observational analysis is further examined using a general circulation model. Comparison of numerical simulations with and without parameterizing convection clearly indicates that decreases in surface wind speed with SST are a result of the interaction of convection with the large-scale circulation. Without convection, wind speed remains essentially constant with SST, and surface latent heat flux increases with SST. The rate of increase is close to what one expects from thermodynamic considerations alone. When convection is parameterized, variations of wind speed, humidity deficit, and latent heat flux with SST are very similar to those observed.

The results of this study have important implications to the role of surface evaporation in regulating SST in the western Pacific warm pool region. If SST were to increase due to some external forcing, such as the super greenhouse effect of the atmosphere, evaporation might not increase in response to the SST change due to suppressed surface wind speeds. Hence, evaporative cooling may not provide the negative feedback required to restore SST.

Finally, it should be pointed out that the findings and conclusions from this study are based on the data from the equatorial Pacific; their applicability to other world oceans, such as the Indian Ocean and the Atlantic, is not clear. It would be useful to extend similar analyses to these oceans. Thus, high quality observational data from these regions are much desired.

Acknowledgments. This research was supported by the Environmental Sciences Division of U.S. Department of Energy under Grant DEFG 0391 ER 61198 (GJZ and VR) as part of the Atmospheric Radiation Measurement Program and NOAA's Equatorial Pacific Ocean Climate Studies Program and the U.S. TOGA Project Office (MJM). We would like to thank the reviewers for their helpful comments.

REFERENCES

Arking, A., and D. Ziskin, 1994: Relationship between clouds and sea surface temperatures in the western tropical Pacific. *J. Climate,* **7,** 988–1000.

Cornejo-Garrido, A. G., and P. H. Stone, 1977: On the heat balance of the Walker circulation. *J. Atmos. Sci.,* **34,** 1155–1162.

Freitag, H. P., Y. Feng, L. J. Mangum, M. J. McPhaden, J. Neander, and L. D. Stratton, 1994: Calibration procedures and instrumental accuracy estimates of TOGA-TAO temperature, relative humidity and radiation measurements. NOAA Tech. Memo. ERL PMEL-104, 32 pp.

Gaynor, J. E., and C. F. Ropelewski, 1979: Analysis of the convectively modified GATE boundary layer using in-situ and acoustic sounder data. *Mon. Wea. Rev.,* **107,** 985–993.

Gill, A. E. 1980: Some simple solutions for heat-induced tropical circulation. *Quart. J. Roy. Meteor. Soc.,* **106,** 447–462.

Graham, N. E., and T. P. Barnett, 1987: Observations of sea surface temperature and convection over tropical oceans. *Science,* **238,** 657–659.

Hartmann, D. L., and M. L. Michelsen, 1993: Large-scale effects on the regulation of tropical sea surface temperature. *J. Climate,* **6,** 2049–2062.

Johnson, R. H., 1981: Large-scale effects of deep convection on the GATE tropical boundary layer. *J. Atmos. Sci.,* **111,** 2399–2413.

Kessler, W. S., and M. J. McPhaden, 1995: The 1991–93 El Nino in the central Pacific. *Deep-Sea Res.,* **42,** 295–333.

Lau, K. M., and C. H. Sui, 1993: Studying radiation, cloud and dynamics feedback processes using cloud-resolving cumulus ensemble models. *Eos* (Suppl), **74**(43), 107.

——, ——, M. D. Chou, and W. K. Tao, 1994: An inquiry into the cirrus-cloud thermostat effect for tropical sea surface temperature. *Geophys. Res. Lett.,* **21,** 1157–1160.

Lindzen, R. S., and S. Nigam, 1987: On the role of sea surface temperature gradients in forcing low level winds and convergence in the tropics. *J. Atmos. Sci.,* **45,** 2440–2458.

Liu, W. T., 1988: Moisture and latent heat flux variabilities in the tropical Pacific derived from satellite data. *J. Geophys. Res.,* **93,** 6749–6760.

——, and C. Gautier, 1990: Thermal forcing on the tropical Pacific from satellite data. *J. Geophys. Res.,* **95,** 13 209–13 217.

——, K. B. Katsaros, and J. A. Businger, 1979: Bulk parameterization of air–sea exchanges of heat and water vapor including molecular constraints at the interface. *J. Atmos. Sci.,* **36,** 1722–1735.

Mangum, L. J., H. P. Freitag, and M. J. McPhaden, 1994: TOGA-TAO array sampling schemes and sensor evaluations. *Proc. OCEANS '94 OSATES,* Vol. 2, Parc de Penfeld, Brest, France, IEEE, 402–406.

McPhaden, M. J., 1993: TOGA-TAO and the 1991–93 ENSO event. *Oceanography,* **6,** 36–44.

——, and S. P. Hayes, 1991: On the variability of winds, sea surface temperature, and surface layer heat content in the western equatorial Pacific. *J. Geophys. Res.,* **96,** 3331–3342.

Parsons, D., and Coauthors, 1994: The integrated sounding systems: Description and preliminary observations from TOGA COARE. *Bull. Amer. Meteor. Soc.,* **75,** 553–567.

Ramanathan, V., and W. Collins, 1991: Thermodynamic regulation of ocean warming by cirrus clouds deduced from observations of the 1987 El Niño, *Nature,* **351,** 27–32.

Reynolds, R. W., and T. M. Smith, 1994: Improved global sea surface temperature analyses using optimum interpolation. *J. Climate,* **7,** 929–948.

Roeckner, E., and Coauthors, 1992: Simulation of the present-day climate with the ECHAM model: Impact of model physics and resolution. Max–Planck–Institute for Meteorology, Rep. 15, Hamburg, Germany, 171 pp.

Thiele, O. W., M. J. McPhaden, and D. A. Short, 1994: Optical rain-gauge performance. *Proc. Second Workshop on Optical Rain-gauge Measurements,* NASA Conf. Publ. 3288, 76 pp.

Waliser, D. E., and N. E. Graham, 1993: Convective cloud systems and warm-pool sea surface temperatures: Coupled interactions and self-regulation. *J. Geophys. Res.,* **98,** 12 881–12 893.

——, ——, and C. Gautier, 1993: Comparison of the highly reflective cloud and outgoing longwave datasets for use in estimating tropical deep convection. *J. Climate,* **6,** 331–353.

Wallace, J. M., 1992: Effect of deep convection on the regulation of tropical sea surface temperature. *Nature,* **357,** 230–231.

Wang, B., and T. Li, 1993: A simple tropical atmosphere model of relevance to short-term climate variations. *J. Atmos. Sci.*, **50**, 260–284.

Young, G. S., D. V. Ledvina, and C. W. Fairall, 1992: The influence of precipitating convection on the surface energy budget observed during a Tropical Ocean Global Atmosphere pilot cruise in the tropical western Pacific Ocean. *J. Geophys. Res.*, **97**, 9595–9603.

Zhang, C., 1993: Large-scale variability of atmospheric deep convection in relation to sea surface temperature in the tropics. *J. Climate*, **6**, 1898–1913.

Zhang, G. J., 1994: Effects of cumulus convection on the simulated monsoon circulation in a general circulation model. *Mon. Wea. Rev.*, **122**, 2022–2038.

——, and N. A. McFarlane, 1995: Sensitivity of climate simulations to the parameterization of cumulus convection in the Canadian Climate Centre general circulation model. *Atmos.–Ocean*, **33**, 407–446.

——, and M. J. McPhaden, 1995: The relationship between sea surface temperature and latent heat flux in the equatorial Pacific. *J. Climate*, **8**, 589–605.